Green synthesis of Ag and Pd nanoparticles for water pollutants treatment

C. Joseph Kirubaharan, Zhen Fang, Chong Sha and Yang-Chun Yong

ABSTRACT

Silver (Ag) and palladium (Pd) nanoparticles were synthesized via a green synthesis route, which was mediated with the extract of *Daucus carota* leaves. The morphological, crystalline and structural nature of the synthesized nanoparticles was characterized by UV-Vis spectrophotometer, and TEM, XRD and FT-IR analyses. High antibacterial activities of the prepared Ag and Pd nanoparticles were observed towards different water-borne pathogens of *Klebsiella pneumonia*, *Vibrio cholera and Escherichia coli*. The catalytic efficiency of the prepared nanoparticles for the removal of rhodamine 6G (Rh-6G) dye was also evaluated. Nearly 98% of the Rh-6G dye was decolorized by the synthesized Pd nanoparticles within 2 min, and the synthesized Ag nanoparticles took 30 min for 89.4% decolorization. This work provided greener nanocatalysts for pollutant treatment and demonstrated the power of green biosynthesis for metallic nanoparticles.

Key words | antibacteria, dye removal, green synthesis, nanoparticles, water pollution

C. Joseph Kirubaharan
Zhen Fang
Chong Sha
Yang-Chun Yong (corresponding author)
Biofuels Institute, School of Environment and Safety Engineering,
Jiangsu University,
301 Xuefu Road, Zhenjiang 212013,
China
E-mail: *ycyong@ujs.edu.cn*

HIGHLIGHTS

- Green approach to synthesis of Ag and Pd nanoparticles was developed.
- The synthesized nanoparticles showed high antibacterial activity.
- These nanoparticles also exhibited excellent catalytic activity for rhodamine removal.

INTRODUCTION

Synthetic dyes from industries cause severe water pollution, which causes serious environmental problems (Zhao *et al.* 2004). Most of the dyes are very harmful contaminants for water sources due to their toxicity and carcinogenic effects (Rasheed *et al.* 2019) and commonly result in severe problems such as inhibiting the growth of microorganisms, reducing light penetration, and increasing chemical oxygen demand (COD). An enormous amount of dyes has been discharged in recent years, which affects the water resources, soil fertility and aquatics to a great extent (Fan *et al.* 2018; Perez-Rodriguez *et al.* 2018). So, it is urgent to develop a strategy to manage the dyes pollution (Kramer *et al.* 2018).

Hence, there are numerous methods such as ozonation, membrane filtration, and electrochemical/photochemical degradation, biodegradation that have been developed for dye removal from water (Kariyajjanavar *et al.* 2010; Krejčíková *et al.* 2012; Zhang *et al.* 2014). However, the aforementioned techniques exhibit certain limitations such as formation of hazardous by-products, high cost, low efficiency or regeneration difficulties (Shen *et al.* 2001; Nawahwi *et al.* 2013; Singh *et al.* 2015). These limitations were effectively tackled by the nanostructured materials through their unique characteristics such as high surface area and electron communication features, narrow band gap, chemical stability, and favorable optoelectronic and light absorbing ability (Dong *et al.* 2013; Yusoff *et al.* 2013).

Nanostructured metals are of great interest due to their widespread applications in modern society (Moores & Goettmann 2006; Cepriá *et al.* 2016; Luo *et al.* 2016; Celania & Mudring 2019). The ultimate aim of the utilization of nanoparticle-mediated dye degradation is to decrease toxicity in the environment (Safari-Amiri *et al.* 2017).The nanoparticles such as NiO, TiO_2, ZnO, ZnS and metal ion-doped titania were utilized for organic dye degradations such as orange-II, reactive black, methyl orange and methylene blue (Ge *et al.* 2009; Saggioro *et al.* 2011; Bonyadinejad *et al.* 2012;

doi: 10.2166/wst.2020.498

Liu *et al.* 2013). However, the synthesized nanoparticles from physical and chemical methods are not environmental friendly due to the usage of hazardous reduction and stabilization agents, which may lead to some adverse effects.

To decrease the utilization of hazardous reduction and stabilization agents, bio-mediated synthesis using microorganisms, plants and algae has been proposed. Recently, the gaseous pollutant acetaldehyde was effectively degraded by *Jatropha curcas*-mediated cerium oxide (CeO_2) (Magudieswaran *et al.* 2018). *Carica papaya* extract was utilized for the preparation of copper oxide (CuO) nanoparticles, and has been used for degradation of coomassie brilliant blue dye (Sankar *et al.* 2014). Especially, Ag and Pd nanoparticles could be synthesized by bio-mediated process and were effectively utilized to degrade the environmental pollutant. For example, bio-mediated Ag nanoparticles were effectively applied for removal of azo dyes (Reddy *et al.* 2018; Rasheed *et al.* 2019). Non-toxic and renewable *Boswellia serrata*-mediated Pd nanoparticles were utilized for the degradation of anthropogenic dye pollutants (Kora & Rastogi 2016).

Among the existing dyes in the xanthene family, rhodamine 6G (Rh-6G) has extensive applications as a dyeing agent, non-linear optical chemical and photosensitizer material (Saini *et al.* 2005; Khalfaoui *et al.* 2012). It has been experimentally proven that Rh-6G exhibits carcinogenic effects and neurotoxicity, which are detrimental to humans and animals (Aarthi & Madras 2007; Lutic *et al.* 2012) Nanoparticles catalyzed photo-degradation was considered to be a promising approach for Rh-6G removal (Carreño *et al.* 2008; Nagaraja *et al.* 2012). Thus, development of green photocatalysts for Rh-6G removal is important. Here, we developed a green method to use *Daucus carota* leaves extracts as the ecofriendly reducing agent for synthesis of Ag nanoparticles (D-Ag) and Pd nanoparticles (D-Pd). Moreover, the catalytic activity for Rh-6G removal and antibacterial activity by these green synthesized nanoparticles were also evaluated.

EXPERIMENTAL

Materials

Daucus carota leaves were obtained from a local supermarket (Zhenjiang, Jiangsu province, China). Silver nitrate ($AgNO_3$), palladium chloride ($PdCl_2$), sodium borohydride ($NaBH_4$) and rhodamine 6G (Rh-6G) were obtained from Aldrich Chemicals. The leaves of *Daucus carota* were obtained from the local premises.

Preparation of *Daucus carota* leave extract

The freshly derived *Daucus carota* leaves were washed and chopped into small pieces (~1 cm × 1 cm). For the preparation of 20 wt. % extract (20 g of *Daucus carota* leaves in 100 ml de-ionized water), an appropriate amount of *Daucus carota* leaves was boiled in de-ionized water at 80 °C for 10 min. Then the solution was filtered by using a Whatman filter paper (no. 1) and the filtrate was considered as the *Daucus carota* leave extract and stored at 4 °C for further use.

Synthesis of D-Ag/D-Pd nanoparticles

Daucus carota extract (20 wt %) was gradually added into the aqueous solution of $AgNO_3$ (1 mM) and the mixture was magnetically stirred for 30 min. The color change was observed from yellow to brown, which suggests the formation of D-Ag nanoparticles (Raouf *et al.* 2019). Similarly, D-Pd nanoparticles were prepared by using an aqueous solution of $PdCl_2$ (1 mM) containing *Daucus carota* extract (20 wt %). Finally, the solution turns a pale yellow color, which suggests the formation of D-Pd nanoparticles (Kettemann *et al.* 2015).

Catalytic reduction of Rh-6G

The catalytic activity of D-AgNPs and D-PdNPs was examined by analyzing the UV–Vis spectra of Rh-6G dye on treatment with sodium borohydride. The concentration of Rh-6G dye was monitored by using the UV-Vis spectrophotometric method (Kalaiselvi *et al.* 2015). Typically, 0.5 ml of dye solution (10 μM) was added to an equal volume of sodium borohydride (0.1M) solution. Then 0.1 ml of the D-Ag NPs solution was added to a mixture of dye and $NaBH_4$, and stirring was continued for an additional 5 min. Absorbance value was continuously monitored during the dye degradation process in UV–Vis spectra at respective wavelengths at room temperature. Additionally, the control reactions were also carried out in parallel without NPs. Similarly, D-Pd NPs were analyzed for the degradation study.

Characterizations

The surface plasmon resonance of the prepared nanoparticles and catalytic Rh-6G dye degradation were monitored by using a UV-Vis spectrophotometer. The crystalline character of the synthesized D-Ag and D-Pd nanoparticles was ascertained by X-ray powder diffractometer (XRD) (Rigaku D/max-2500). Morphological images and dimensions of

the prepared nanoparticles were evaluated by using a JEOL JEM-2010 transmission electron microscope. Structural characterization of the prepared nanoparticles was examined using a Perkin Elmer Fourier transform infrared (FT-IR) spectroscopy in KBr pellets.

Antibacterial activity

The antibacterial activity of D-Ag and D-Pd nanoparticles was analysed with three different bacterial cultures such as *Klebsiella pneumonia, Vibrio cholerae* and *Escherichia coli* by zone inhibition method compare with ampicillin as a positive control. Initially, the bacterial inoculums were placed on the petri plates by using an L-rod and making the wells for the analysis. Then, synthesized nanoparticles (50 μg/ml) were poured into wells and the plates were incubated at 37 °C in an aerobic incubation chamber. After 24 h incubation, the inhibition zone was observed and the diameter was measured. Furthermore, the antibacterial activities of D-Ag and D-Pd nanoparticles towards the *Escherichia coli* (1×10^5 CFU/ml) were also analyzed using the plate counting method. An equal volume from the bacterial cell and nanoparticles suspension was mixed in sterile tubes and incubated for 3 h at 37 °C. Subsequently, each suspension was plated on LB agar plate, incubated for 16 h at 37 °C, and the CFU was analyzed. The antibacterial percentage was calculated according to Equation (1), in this case A_0 is the number of bacterial colonies in control without nanoparticles, and A_i is the surviving bacterial colonies after interaction with nanoparticles:

$$\text{Antibacterial activity}\,(\%) = A_0 - A_i/A_0 \times 100 \quad (1)$$

RESULTS AND DISCUSSION

Characterization of Ag and Pd nanoparticles synthesized by green approach

To evaluate the possibility to synthesize D-Ag and D-Pd nanoparticles with *Daucus carota* leaf extracts, the color change of the solution during synthesis was monitored and the synthesized product was characterized. After addition of the extract into $AgNO_3$ or $PdCl_2$ solution, the solution gradually changed to brown and pale yellow color, suggesting the reduction of $AgNO_3$ or $PdCl_2$ had occurred, respectively (Figure 1).

The formation of D-Ag nanoparticles was confirmed by UV-Vis spectrum, which shows a sharp absorption band at 393 nm (Figure 2(a)). By adjusting the pH of the solution (pH = 6) to basic medium (pH = 9), the color of the nanoparticles was further intensified and attributed in the variation of dissociation constant (pKa) of the functional groups, which is attached on the phyto-chemicals of the biomass (Mukherjee *et al.* 2001; Vigneshwaran *et al.* 2006; Silva *et al.* 2007; Wang *et al.* 2018). Biomass of the extract is helpful for reduction and stabilization of nanoparticles and the inclusion of sodium hydroxide (pH = 9) sharpened the SPR band, which indicates the reduction in dimension of the prepared nanoparticles. The incorporation of aqueous *Daucus carota* extract is responsible for the formation of D-Pd nanoparticles, identified by the vanished SPR band at 400 nm, and the colour of the solution becomes pale yellow (Figure 2(b)).

Morphological structures of synthesized D-Ag and D-Pd nanoparticles were discussed with TEM images (Figure 3(a)). Most of the nanoparticles were formed as spherical in shape

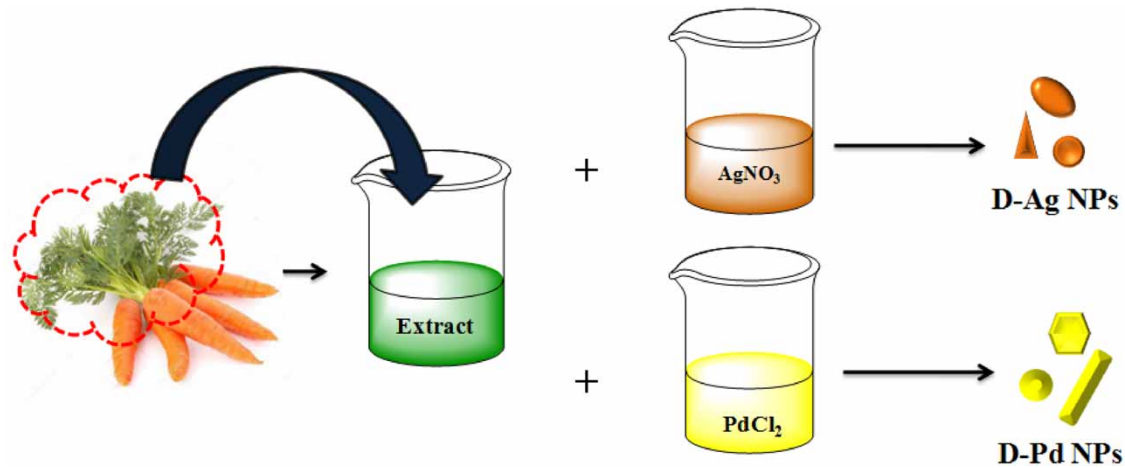

Figure 1 | Schematic for the formation of D-Ag and D-Pd nanoparticles.

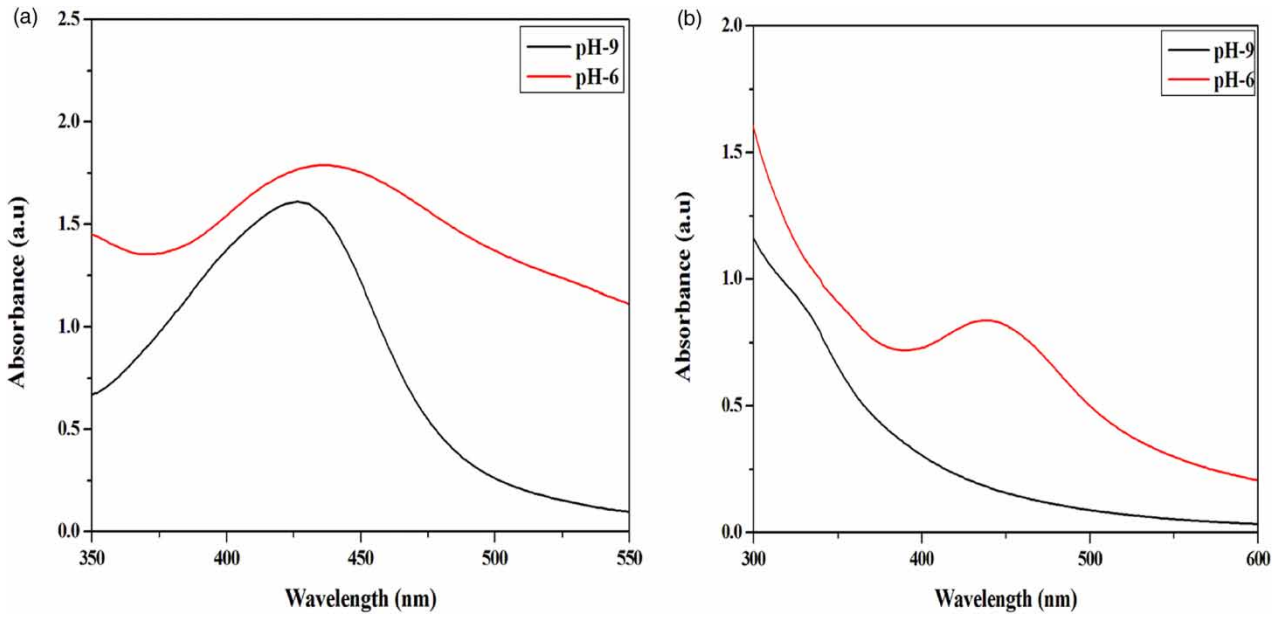

Figure 2 | UV-Vis absorption spectrum of the (a) D-Ag and (b) D-Pd nanoparticles with different pH.

and of different sizes with a smooth surface. In addition to the spherical-shaped nanoparticles, the triangular shape of D-Ag nanoparticles was also observed from the morphological images. The average size of the D-Ag nanoparticles was obtained as in the range of 18–25 nm and the diameter of the triangle shaped nanoparticles was around 40–50 nm (Celebioglu *et al.* 2019). Rod like structures of D-Pd were clearly observed from the morphological images and the diameter of D-Pd nanoparticles was in the range of 20 nm and the length of the nanoparticles varied from 38–48 nm (Figure 3(b)) (Nadagouda & Varma 2008).

The crystalline nature of D-Ag and D-Pd nanoparticles was further confirmed by X-ray diffraction (XRD) pattern, respectively (Figure 4(a)). The index peaks were observed at angles of 38.1°, 46.2°, 64.5° and 76.8° and can be assigned to (111), (200), (220), and (311) reflections, respectively (Wen *et al.* 2006). It confirms the pure crystalline nature and fcc (face-centered cubic) structure of the synthesized nanometric D-Ag. The highly crystalline nature of D-Pd nanoparticles was confirmed from the highly intensified peaks observed at the angles of 39°, 45.5°, 64.3°, 81.2° and 83.6° and can be assigned to (111), (200), (220), (311) and (222)

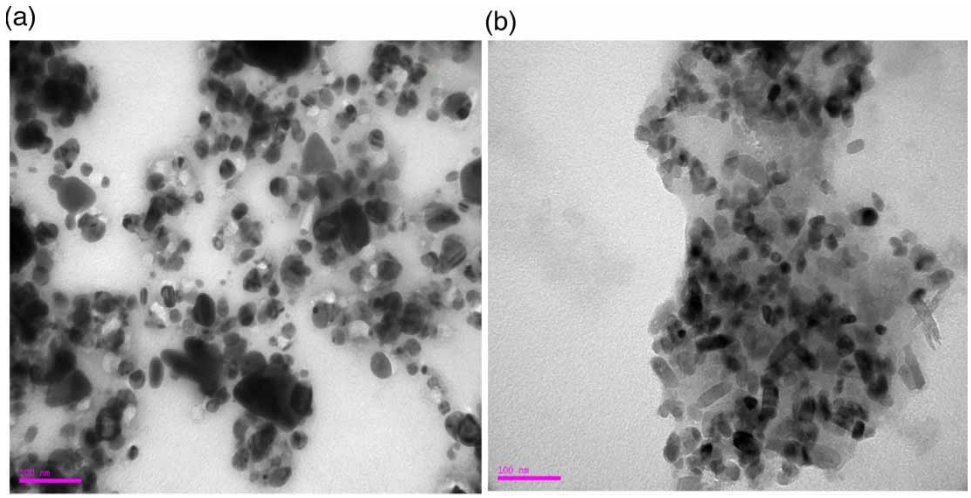

Figure 3 | TEM images of the (a) D-Ag and (b) D-Pd nanoparticles.

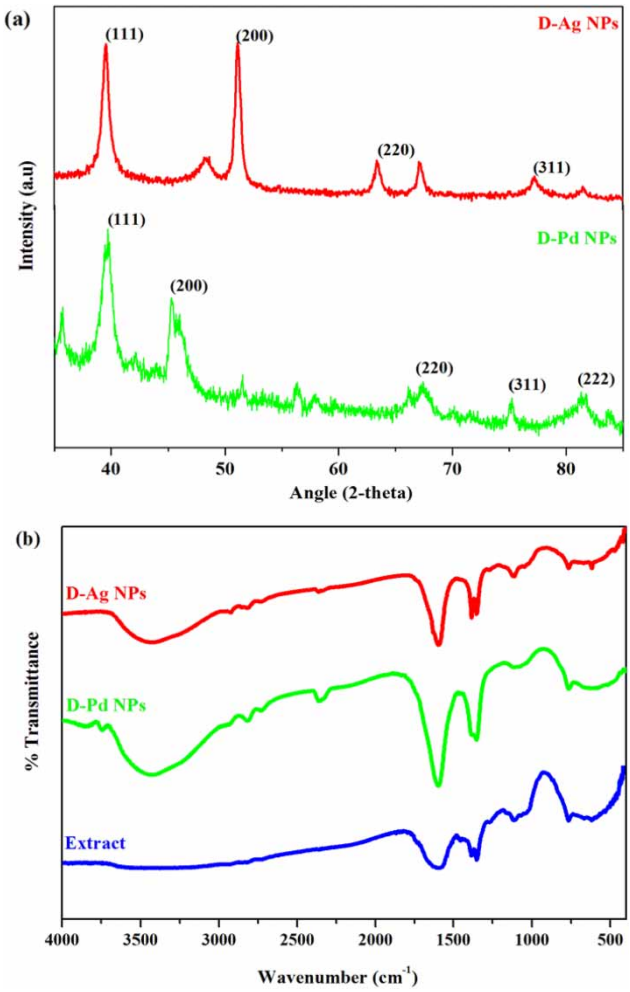

Figure 4 | (a) XRD spectrum of the D-Ag and D-Pd nanoparticles. (b) FT-IR spectra of the D-Ag, D-Pd and *Daucus carota* extract.

respectively (Yang *et al.* 2010). A characteristic crystalline peak observed in the XRD pattern is attributed to the crystalline nature of the biomass.

FT-IR spectra of the synthesized D-Ag and D-Pd nanoparticles were analyzed with plausible functional groups (Figure 4(b)). FT-IR spectrum of prepared nanoparticles showed intensive bands at 3,434, 2,358 cm^{-1} that were attributed to N-H and C = O stretching vibrations, respectively (Prathna *et al.* 2011). In generally, 1,379 cm^{-1} is assigned to the germinal methyl groups and the mentioned band has shifted to 1,384 cm^{-1}. Bio-mediated nanoparticle peaks were located around 1,598 cm^{-1} and attributed to C = C stretching (Tripathy *et al.* 2010). From the analysis, it is clear that the flavanones and terpenoids could have appeared on the metal nanoparticle surface by a possible interaction via carbonyl groups. Reducing sugar and terpenoids were helpful for the π bond formation on the carbonyl group in biosynthesized nanoparticles. Physiosorbed functional groups may cause electrostatic or steric walls around the surface of bio-mediated nanoparticles to provide stabilization of nanoparticles, which may improve their catalytic performance for antibacterial or dye decolorization (Rasheed *et al.* 2018).

Antibacterial activity of the synthesized Ag and Pd nanoparticles

It is well known that Ag or Pd nanoparticles have good antibacterial activity. The antimicrobial action of Ag^{+} and Pd^{+} is closely associated with the interface with sulfhydryl groups in enzymes and proteins. For instance, Ag^{+} and Pd^{+} can bind to proteins that are present in the cell membrane to form stable bonds, resulting in protein deactivation, which would be detrimental to bacterial cells (Klueh *et al.* 2000; Giessen & Silver 2016). Antibacterial activities for the D-Ag and D-Pd nanoparticles were tested against *Klebsiella pneumonia, Vibrio cholera and Escherichia coli* and the activity compared by the zone of inhibition method (ZOI) (Figure S1 in Supplementary Material). From the results, the antibacterial activity of D-Ag and D-Pd nanoparticles against *Klebsiella pneumonia* (ZOI = 36 mm for D-AgNPs, 24 mm for D-PdNPs) and *Vibrio cholera* (ZOI = 44 mm for D-AgNPs, 18 mm for D-PdNPs) was higher than against *Escherichia coli* (ZOI = 18 mm for D-AgNPs, 16 mm for D-PdNPs). In this study, D-Ag nanoparticles have good antibacterial behavior towards Gram-negative bacteria stains with the same concentration. Also, the synthesized D-Pd nanoparticles have shown an obvious inhibition zone against the tested microorganisms and the observed activity was similar to the D-Ag nanoparticles. Furthermore, antibacterial activity of prepared nanoparticles was evaluated by the colony-forming unit (CFU) method with different concentrations against Gram–negative *Escherichia coli* for 16 h of incubated time at 37 °C. The maximum antibacterial activities for D-Ag and D-Pd nanoparticles were around 88.9% and 92.7% at 1,200 μg/ml respectively (Figure 5). The results indicated that the synthesized nanoparticles with *Daucus carota* extracts have good antibacterial activity, which might be used for water disinfection.

Catalytical degradation of Rh-6G by D-Ag and D-Pd nanoparticles

The catalytic efficiency of prepared D-Ag and D-Pd nanoparticles towards the degradation of Rh-6G dye using $NaBH_4$ as the reducing agent was carried out at room temperature. Rh-6G exhibited a characteristic SPR band at 526 nm

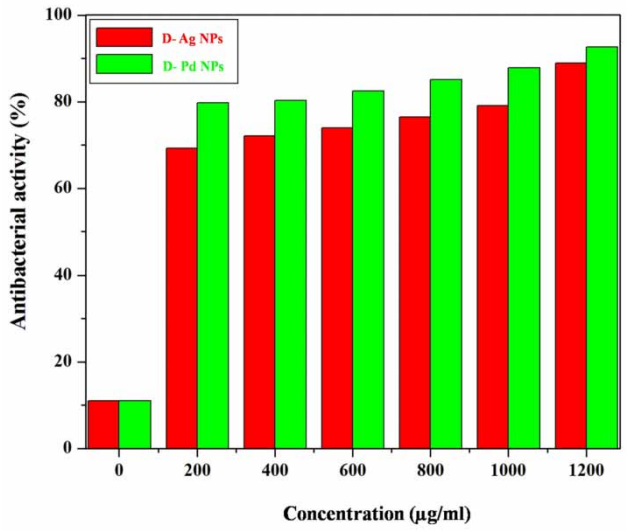

Figure 5 | Antibacterial activity of D-Ag and D-Pd nanoparticles at different concentrations against *Escherichia coli*.

corresponding to characteristic π–π* transition (Bakkialakshmi *et al.* 2012). The degradation of Rh-6G dye by D-Ag and D-Pd nanoparticles with $NaBH_4$ was monitored by UV-Vis absorption spectroscopy.

The intensity of absorptions of Rh-6G was only slightly decreased as a function of time with an addition of $NaBH_4$, which can be explained by the electrons from $NaBH_4$ being transferred to the Rh-6G molecule and reducing the dye molecules (Song *et al.* 2014). However, the dye degradation process was saturated at 30 min with minimal degradation by $NaBH_4$ (Figure 6(a)). The addition of *Daucus carota* extract decreased the UV-Vis adsorption of the dye molecule, and may be ascribed to the dilution effect (Figure 6(b)). Then, the D-Ag and D-Pd nanoparticles synthesized with *Daucus carota* extract were used as the catalyst for Rh-6G reduction with $NaBH_4$. Although the color intensity of Rh-6G dye was decreased as a function of time, complete decolorization was not observed for D-Ag nanoparticles (Figure 6(c)). However, the addition of D-Pd nanoparticles completely removed Rh-6G within 2 min (Figure 6(d)). The change in the color of the dye was monitored up to 30 min to confirm the removal efficiency of D-Pd nanoparticles, revealing the independence of dye reduction from adsorption. According to the reduction profile, $NaBH_4$ reduced 30% of dye with at maximum ability. D-Ag nanoparticles exhibited a gradual degradation and reduced 89% of dye, which explains the change in initial

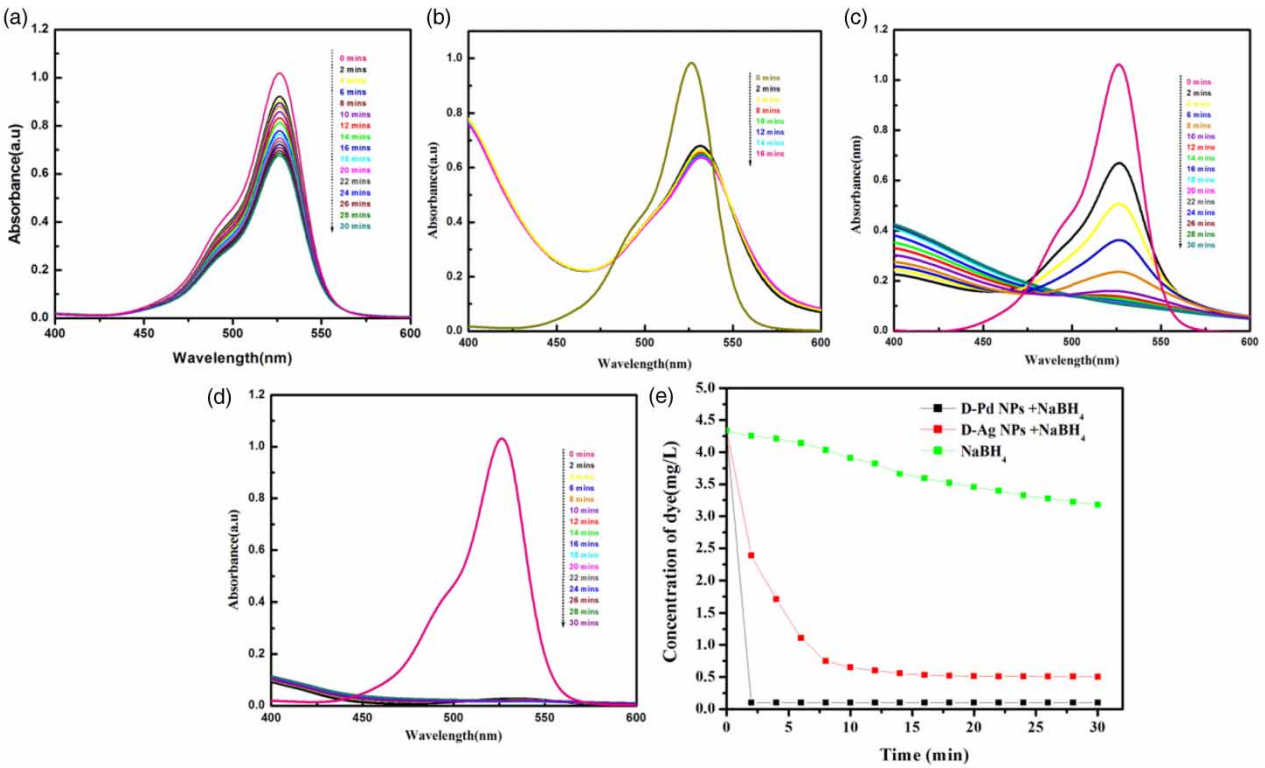

Figure 6 | UV-Vis absorption spectra of Rh-6G in presence of (a) $NaBH_4$, (b) $NaBH_4$ with *Daucus carota* extract (c) $NaBH_4$ with D-Ag and (d) $NaBH_4$ with D-Pd nanoparticles. (e) Time course profiles of Rh-6G reduction.

concentration of dye with function of time. Similarly, the concentration of Rh-6G dye rapidly decreased in the presence of $NaBH_4$ mediated D-Pd nanoparticles reduced 98% of dye within 2 min and the degradation rate was much higher than the Ag nanoparticles (Figure 6(e)). These results substantiated that these nanoparticles synthesized with the developed green method could be applied for catalytic water pollution treatment.

CONCLUSION

D-Ag and D-Pd nanoparticles were synthesized using *Daucus carota* leaves mediated bio-synthesis process. *Daucus carota* broth extract acts as an effective reducing and stabilizing agent in the preparation of nanoparticles and was examined by FTIR analysis. The synthesized nanoparticles were effectively applied in the degradation process for the cost-effective removal of pollutants. The catalytic decolorization of Rh-6G dye and pathogen deactivation was achieved with D-Ag and D-Pd nanoparticles synthesized with the green method. These findings prove that *Daucus carota* extracts could be an eco-friendly reducing agent for functional nanoparticle synthesis. The plant-extract based nanoparticles showed the advantages of cheap, environmentally friendly, self-capping and stabilization, which would be useful for practical application in water pollutant management.

ACKNOWLEDGEMENT

This work was supported by the Priority Program Development of Jiangsu Higher Education Institutions (China).

DATA AVAILABILITY STATEMENT

All relevant data are included in the paper or its Supplementary Information.

REFERENCES

Aarthi, T. & Madras, G. 2007 Photocatalytic degradation of rhodamine dyes with nano-TiO_2. *Industrial & Engineering Chemistry Research* **46** (1), 7–14.

Bakkialakshmi, S., Selvarani, P. & Chenthamarai, S. 2012 Absorption characterization of a dye and two amines. *Archives of Applied Science Research* **4**, 150–154.

Bonyadinejad, G., Amin, M., Mohammadi, H. & Nateghi, R. 2012 Decolorization of synthetic wastewaters by nickel oxide nanoparticle. *International Journal of Environmental Health Engineering* **1**, 25.

Carreño, N. L. V., Garcia, I. T. S., Carreño, L. S. S. M., Nunes, M. R., Leite, E. R., Fajardo, H. V. & Probst, L. F. D. 2008 Synthesis of titania/carbon nanocomposites by polymeric precursor method. *Journal of Physics and Chemistry of Solids* **69** (8), 1897–1904.

Celania, C. & Mudring, A.-V. 2019 Structures, properties, and potential applications of rare earth-noble metal tellurides. *Journal of Solid State Chemistry* **274**, 243–258.

Celebioglu, A., Topuz, F. & Uyar, T. 2019 Facile and green synthesis of palladium nanoparticles loaded into cyclodextrin nanofibers and their catalytic application in nitroarene hydrogenation. *New Journal of Chemistry* **43** (7), 3146–3152.

Cepriá, G., Pardo, J., Lopez, A., Peña, E. & Castillo, J. 2016 Selectivity of silver nanoparticle sensors: discrimination between silver nanoparticles and Ag^+. *Sensors and Actuators B: Chemical* **230**, 25–30.

Dong, P., Wang, Y., Cao, B., Xin, S., Guo, L., Zhang, J. & Li, F. 2013 Ag_3PO_4/reduced graphite oxide sheets nanocomposites with highly enhanced visible light photocatalytic activity and stability. *Applied Catalysis B: Environmental* **132–133**, 45–53.

Fan, J., Chen, D., Li, N., Xu, Q., Li, H., He, J. & Lu, J. 2018 Adsorption and biodegradation of dye in wastewater with Fe_3O_4@MIL-100 (Fe) core–shell bio-nanocomposites. *Chemosphere* **191**, 315–323.

Ge, M., Guo, C., Zhu, X., Ma, L., Han, Z., Hu, W. & Wang, Y. 2009 Photocatalytic degradation of methyl orange using ZnO/TiO_2 composites. *Frontiers of Environmental Science & Engineering in China* **3** (3), 271–280.

Giessen, T. W. & Silver, P. A. 2016 Converting a natural protein compartment into a nanofactory for the size-constrained synthesis of antimicrobial silver nanoparticles. *ACS Synthetic Biology* **5** (12), 1497–1504.

Kalaiselvi, A., Roopan, S. M., Madhumitha, G., Ramalingam, C. & Elango, G. 2015 Synthesis and characterization of palladium nanoparticles using *Catharanthus roseus* leaf extract and its application in the photo-catalytic degradation. *Spectrochima Acta Part A* **135**, 116–119.

Kariyajjanavar, D. P., Narayana, J., Nayaka, Y. A. & Umanaik, M. 2010 Electrochemical degradation and cyclic voltammetric studies of textile reactive azo dye Cibacron Navy WB. *Portugaliae Electrochimica Acta* **28**, 265.

Kettemann, F., Wuithschick, M., Caputo, G., Kraehnert, R., Pinna, N., Rademann, K. & Polte, J. 2015 Reliable palladium nanoparticle syntheses in aqueous solution: the importance of understanding precursor chemistry and growth mechanism. *Crystal Engineering Communication* **17**, 1865–1870.

Khalfaoui, N., Boutoumi, H., Khalaf, H., Oturan, N. & A. Oturan, M. 2012 Electrochemical oxidation of the xanthene dye Rhodamine 6G by electrochemical advanced oxidation using Pt and BDD anodes. *Current Organic Chemistry* **16** (18), 2083–2090.

Klueh, U., Wagner, V., Kelly, S., Johnson, A. & Bryers, J. D. 2000 Efficacy of silver-coated fabric to prevent bacterial colonization and subsequent device-based biofilm formation. *Journal of Bio Medicinal Material Research* **53** (6), 621–631.

Kora, A. J. & Rastogi, L. 2016 Catalytic degradation of anthropogenic dye pollutants using palladium nanoparticles synthesized by gum olibanum, a glucuronoarabinogalactan biopolymer. *Industrial Crops and Products* **81**, 1–10.

Kramer, S., Hejjo, F., Rasmussen, K. H. & Kegnæs, S. 2018 Silylative pinacol coupling catalyzed by nitrogen-doped carbon-encapsulated nickel/cobalt nanoparticles: evidence for a silyl radical pathway. *ACS Catalysis* **8** (2), 754–759.

Krejčíková, S., Matějová, L., Kočí, K., Obalová, L., Matěj, Z., Čapek, L. & Šolcová, O. 2012 Preparation and characterization of Ag-doped crystalline titania for photocatalysis applications. *Applied Catalysis B: Environmental* **111–112**, 119–125.

Liu, F., Guo, M. Y., Leung, Y. H., Djurišić, A. B., Ng, A. M. C. & Chan, W. K. 2013 Effect of starting properties and annealing on photocatalytic activity of ZnO nanoparticles. *Applied Surface Science* **283**, 914–923.

Luo, Y., Li, J. & Huang, J. 2016 Bioinspired hierarchical nanofibrous silver-nanoparticle/anatase–rutile-titania composite as an anode material for lithium-ion batteries. *Langmuir* **32** (47), 12338–12343.

Lutic, D., Coromelci-Pastravanu, C., Cretescu, I., Poulios, I. & Stan, C.-D. 2012 Photocatalytic treatment of rhodamine 6G in wastewater using photoactive ZnO. *International Journal of Photoenergy* **2012**, 475131.

Magudieswaran, R., Ishii, J., Nagamuthu Raja, K. C., Terashima, C., Venkatachalam, R., Fujishima, A. & Sudhagar, P. 2018 Green and chemical synthesized CeO_2 nanoparticles for photocatalytic indoor air pollutant degradation. *Materials Letters* **239**, 40–44.

Moores, A. & Goettmann, F. 2006 The plasmon band in noble metal nanoparticles: an introduction to theory and applications. *New Journal of Chemistry* **30** (8), 1121–1132.

Mukherjee, P., Ahmad, A., Mandal, D., Senapati, S., Sainkar, S. R., Khan, M. I., Parishcha, R., Ajaykumar, P. V., Alam, M., Kumar, R. & Sastry, M. 2001 Fungus-mediated synthesis of silver nanoparticles and their immobilization in the mycelial matrix: a novel biological approach to nanoparticle synthesis. *Nano Letters* **1** (10), 515–519.

Nadagouda, M. & Varma, R. 2008 Green synthesis of silver and palladium nanoparticles at room temperature using coffee and tea extract. *Green Chemistry* **10**, 859–862.

Nagaraja, R., Kottam, N., Girija, C. R. & Nagabhushana, B. M. 2012 Photocatalytic degradation of Rhodamine B dye under UV/solar light using ZnO nanopowder synthesized by solution combustion route. *Powder Technology* **215–216**, 91–97.

Nawahwi, M. Z., Ibrahim, Z. & Yahya, A. 2013 Degradation of the Azo Dye reactive Red 195 by *Paenibacillus* spp. R2. *Journal of Bioremediation & Biodegradation* **4**, 174.

Perez-Rodriguez, P., Maqueira Gonzalez, C., Bennani, Y., Rietveld, L. C., Zeman, M. & Smets, A. H. M. 2018 Electrochemical oxidation of organic pollutants powered by a silicon-based solar cell. *ACS Omega* **3** (10), 14392–14398.

Prathna, T. C., Chandrasekaran, N., Raichur, A. M. & Mukherjee, A. 2011 Biomimetic synthesis of silver nanoparticles by *Citrus limon* (lemon) aqueous extract and theoretical prediction of particle size. *Colloids and Surfaces. B, Biointerfaces* **82** (1), 152–159.

Raouf, N. A., Al-Enazi, N. M., Ibraheem, I. B. M., Alharbi, R. M. & Alkhulaifi, M. M. 2019 Biosynthesis of silver nanoparticles by using of the marine brown alga *Padina pavonia* and their characterization. *Saudi Journal of Biological Sciences* **26**, 1207–1215.

Rasheed, T., Bilal, M., Li, C., Nabeel, F., Khalid, M. & Iqbal, H. M. N. 2018 Catalytic potential of bio-synthesized silver nanoparticles using *Convolvulus arvensis* extract for the degradation of environmental pollutants. *Journal of Photochemistry & Photobiology, B: Biology* **181**, 44–52.

Rasheed, T., Bilal, M., Nabeel, F., Adeel, M. & Iqbal, H. M. N. 2019 Environmentally-related contaminants of high concern: potential sources and analytical modalities for detection, quantification, and treatment. *Environment International* **122**, 52–66.

Reddy, J., Mata, R., Raja, K. & Varshney, K. C. 2018 Green synthesized silver nanoparticles: catalytic dye degradation, in vitro anticancer activity and in vivo toxicity in rats. *Materials Science and Engineering C* **91**, 372–381.

Safari-Amiri, M., Mortazavi-Derazkola, S., Salavati-Niasari, M. & Ghoreishi, S. M. 2017 Synthesis and characterization of Dy_2O_3 nanostructures: enhanced photocatalytic degradation of rhodamine B under UV irradiation. *Journal of Materials Science: Materials in Electronics* **28** (9), 6467–6474.

Saggioro, E. M., Oliveira, A. S., Pavesi, T., Maia, C. G., Ferreira, L. F. V. & Moreira, J. C. 2011 Use of titanium dioxide photocatalysis on the remediation of model textile wastewaters containing azo dyes. *Molecules* **16** (12), 10370–10386.

Saini, G. S. S., Kaur, S., Tripathi, S. K., Mahajan, C. G., Thanga, H. H. & Verma, A. L. 2005 Spectroscopic studies of rhodamine 6G dispersed in polymethylcyanoacrylate. *Spectrochimica Acta Part A: Molecular and Biomolecular Spectroscopy* **61** (4), 653–658.

Sankar, R., Manikandan, P., Malarvizhi, V., Fathima, T., Shivashangari, K. S. & Ravikumar, V. 2014 Green synthesis of colloidal copper oxide nanoparticles using *Carica papaya* and its application in photocatalytic dye degradation. *Spectrochimica Acta Part A: Molecular and Biomolecular Spectroscopy* **121**, 746–750.

Shen, Z., Wang, W., Jia, J., Ye, J., Feng, X. & Peng, A. 2001 Degradation of dye solution by an activated carbon fiber electrode electrolysis system. *Journal of Hazardous Materials* **84** (1), 107–116.

Silva, A. M. B., de Araújo, C. B., Santos-Silva, S. & Galembeck, A. 2007 Silver nanoparticle in situ growth within crosslinked poly(ester-co-styrene) induced by UV irradiation: aggregation control with exposure time. *Journal of Physics and Chemistry of Solids* **68** (5), 729–733.

Singh, R. L., Singh, P. K. & Singh, R. P. 2015 Enzymatic decolorization and degradation of azo dyes – A review. *International Biodeterioration & Biodegradation* **104**, 21–31.

Song, S., Song, A. & Hao, J. 2014 Hexagonal hollow microtubes incorporated Bi_2S_3-quantum-dots for catalytic degradation of dyes. *Journal of Colloid and Interface Science* **413**, 133–139.

Tripathy, A., Raichur, A. M., Chandrasekaran, N., Prathna, T. C. & Mukherjee, A. 2010 Process variables in biomimetic synthesis of silver nanoparticles by aqueous extract of *Azadirachta indica* (Neem) leaves. *Journal of Nanoparticle Research* **12** (1), 237–246.

Vigneshwaran, N., Kathe, A. A., Varadarajan, P. V., Nachane, R. P. & Balasubramanya, R. H. 2006 Biomimetics of silver nanoparticles by white rot fungus, *Phaenerochaete chrysosporium*. *Colloids and Surfaces B: Biointerfaces* **53** (1), 55–59.

Wang, L., Lu, F., Liu, Y., Wu, Y. & Wu, Z. 2018 Photocatalytic degradation of organic dyes and antimicrobial activity of silver nanoparticles fast synthesized by flavonoids fraction of *Psidium guajava* L. leaves. *Journal of Molecular Liquids* **263**, 187–192.

Wen, X., Xie, Y.-T., Mak, W. C., Cheung, K. Y., Li, X.-Y., Renneberg, R. & Yang, S. 2006 Dendritic nanostructures of silver: facile synthesis, structural characterizations, and sensing applications. *Langmuir* **22** (10), 4836–4842.

Yang, X., Li, Q., Wang, H., Huang, J., Lin, L., Wang, W., Sun, D., Su, Y., Opiyo, J. B., Hong, L., Wang, Y., He, N. & Jia, L. 2010 Green synthesis of palladium nanoparticles using broth of *Cinnamomum camphora* leaf. *Journal of Nanoparticle Research* **12** (5), 1589–1598.

Yusoff, N., Huang, N. M., Muhamad, M. R., Kumar, S. V., Lim, H. N. & Harrison, I. 2013 Hydrothermal synthesis of CuO/functionalized graphene nanocomposites for dye degradation. *Materials Letters* **93**, 393.

Zhang, S., Liu, X., Wang, M., Wu, B., Pan, B., Yang, H. & Yu, H.-Q. 2014 Correction to diketone-mediated photochemical processes for target-selective degradation of dye pollutants. *Environmental Science & Technology Letters* **1** (2), 196–196.

Zhao, W., Ma, W., Chen, C., Zhao, J. & Shuai, Z. 2004 Efficient degradation of toxic organic pollutants with $Ni_2O_3/TiO_{2-x}B_x$ under visible light irradiation. *Journal of the American Chemical Society* **126**, 4782–4783.

First received 18 May 2020; accepted in revised form 30 September 2020. Available online 14 October 2020